Anomalous behaviour of the weak exchange coupling between water bibridged dimers in $(9-\mathrm{aminoacridinium})_2\mathrm{CuCl}_4\cdot\mathrm{H_2O}$ crystals. Temperature and pressure EPR studies

1999 J. Phys.: Condens. Matter 11 2437

(http://iopscience.iop.org/0953-8984/11/11/014)

J. Phys.: Condens. Matter **11** (1999) 2437–2448. Printed in the UK PII: S0953-8984(99)98035-9

Anomalous behaviour of the weak exchange coupling between water bibridged dimers in (9-aminoacridinium)$_2$CuCl$_4 \cdot$ H$_2$O crystals. Temperature and pressure EPR studies

S K Hoffmann†§, J Goslar†, W Hilczer†, M Krupski† and L W ter Haar‡

† Institute of Molecular Physics, Polish Academy of Sciences, Smoluchowskiego 17, PL-60179 Poznań, Poland

‡ University of Texas, Department of Chemistry, El Paso, TX 79968-0513, USA

Received 1 October 1998, in final form 2 December 1998

Abstract. Angular, temperature (4.2–300 K) and pressure (0–400 MPa) variations of the EPR spectra of (9-aminoacridinium)$_2$CuCl$_4 \cdot$ H$_2$O single crystals show that magnetic dimers of CuCl$_4$ bibridged by water molecules exist with a triplet state produced by dipolar coupling between Cu^{2+} ions. This is consistent with preliminary structural x-ray diffraction data. Using a decoupling computer procedure the superexchange coupling parameter between dimers was determined as $J_{eff} = 0.0040$ cm^{-1} at room temperature. The parameter depends strongly on temperature and pressure with an anomalous minimum in $J(T)$ at about 200 K. Such behaviour is discussed in terms of a phenomenological model of competing contributions to the effective superexchange coupling based on existing superexchange theories. We have found that the interdimer exchange coupling is antiferromagnetic, and leads to a magnetic ordering at very low temperatures as observed by the huge EPR line broadening.

1. Introduction

The exchange interaction between paramagnetic centres transmitted through atomic pathways (superexchange coupling) has been extensively investigated in relation to magnetism of solids [1]. Experimental and theoretical studies of the superexchange are currently stimulated by searching for high temperature molecular ferromagnets and mechanisms of the fast electron transfer in photosynthesis centres and metalloenzymes. Understanding of the superexchange transmission is still rather qualitative especially for extended molecular bridges. A fundamental superexchange theory proposed by Anderson [2] was based on a concept of potential ferromagnetic (F) exchange and kinetic antiferromagnetic (AF) contributions. Molecular equivalents of the Anderson solid state theory were proposed by Kahn and Briat [3], and Hay *et al* [4]. Also *ab initio* calculations based on Anderson's formalism were performed for model and real dimeric systems [5]. The theoretical works have shown that the phenomenon of superexchange interaction cannot be understood properly in the framework of the 'classical' molecular orbital model without the configuration interaction which is necessary to build the covalency into the wavefunction. An accuracy of theoretical calculations of the various contributions to J is limited by approximations made to limit the size of calculations and the resulting J-value is a small difference of large electronic energies. Thus, still the

§ Author to whom correspondence should be addressed. Fax: (+48-61)868-45-24. E-mail address: skh@ifmpan.poznan.pl.

0953-8984/99/112437+12$19.50

semiempirical Goodenough–Kanamori rules based on the symmetry properties of the metal orbitals reformulated by Anderson [2] are used for a rough evaluation of the strength of the superexchange coupling in real systems.

The problem of magnetostructural correlations studied extensively in strongly exchange-coupled dimers [6] becomes much more complicated in the case of weak long-distance superexchange as we reviewed previously [7]. The smallest superexchange coupling was detected at a distance of 2.5 nm by the EPR method with $J \approx 10^{-4}$ cm^{-1} [7]. In the vast majority of weakly coupled systems the exchange integral was found to be strongly temperature dependent in contradiction to the strongly coupled dimers. Temperature [7] and pressure [8] EPR experiments have shown that the main reason for the temperature variations of J is thermal lattice contraction affecting intermolecular bonds. The problem is complicated by the fact that often a few exchange pathways interfere and various molecular groups such as SO_4, NO_2 and NH_2 involved in a hydrogen bond system have different efficiency for the superexchange transmission.

A special case appears when the H_2O molecule takes part in superexchange transmission since the water molecule is an orthogonality point on the superexchange pathway and favours the ferromagnetic coupling as observed in $Co(en)_2CuCl_5 \cdot H_2O$ [9]. However, in most Cu^{2+} dimers coupled by coordinated water molecules [10–16] antiferromagnetic exchange coupling was found whereas a weak ferromagnetic behaviour was reported for trinuclear units ($J = 0.06$ cm^{-1}) [12] and for $[CuCl(HL)H_2O]_2 \cdot 6H_2O$ ($J = 0.10$ cm^{-1}) [16]. Despite a large collection of experimental data and theoretical studies [17] no general correlation between structural factors and magnitude of superexchange coupling has been found in systems where the coupling is transmitted through hydrogen bonds formed by water molecules.

A different type of hydrogen bonded dimer is presented in this paper. Water molecules are not coordinated to the Cu^{2+} ion but two $CuCl_4^{2-}$ ions are coupled into dimers by two hydrogen bonded H_2O molecules. The dimers are coupled by amino groups of acridine molecules into alternate chains. The $Cu \cdots Cu$ distance within the dimeric unit is 0.730 nm whereas the Cu^{2+} ion from the nearest dimer is located at a distance of 0.784 nm only. Thus, one question is whether the real magnetic dimer with $S = 1$ exists. We will prove it by observation of the zero-field splitting of the EPR lines and analysis of the dipolar and superexchange coupling along the chain. We have found, moreover, that interdimer superexchange is affected by temperature with minimal J-value at about 220 K. It is the first case where superexchange integral J does not decrease or increase monotonically with temperature [7]. This will be discussed based on temperature and pressure EPR data.

2. Experimental details

Single crystals of (9-aminoacridinium)$_2CuCl_4 \cdot H_2O \equiv (Aacr)_2CuCl_4 \cdot H_2O \equiv C_{26}H_{24}Cl_4$ CuN_4O were grown from the aqueous solution of a stoichiometric ratio of 9-aminoacridine $=$ $NH_2C_{13}H_8N$ and cupric chloride. The triclinic crystals grow in the form of red prisms elongated along the [111] direction with well developed $(01\bar{1})$, $(1\bar{1}0)$ and $(\bar{1}01)$ faces. Preliminary x-ray diffraction data [18] show the $P\bar{1}$ crystal symmetry with unit cell dimensions at 298 K: $a = 0.9979(2)$ nm, $b = 1.1869(2)$ nm, $c = 1.3382(2)$ nm, $\alpha = 102.01(1)^\circ$, $\beta = 106.58(1)^\circ$, $\gamma = 113.85(1)^\circ$, $Z = 2$. The crystal structure consists of isolated $CuCl_4^{2-}$-tetrahedra and interspersed planar 9-aminoacridinium cations and H_2O molecules. All of these moieties are linked with each other via weak hydrogen bondings.

The organic sublattices consist of two different pairs of acridinium cations that lie in the same plane, yet each pair is rotated approximately 150° relative to the other pair around the axis perpendicular to the molecular plane. The inorganic sublattice is comprised of $CuCl_4^{2-}$

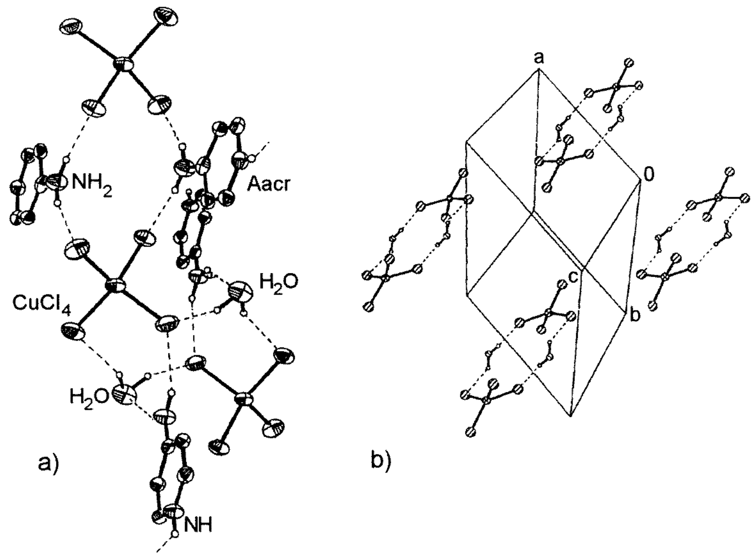

Figure 1. Crystal structure of (9-aminoacridinium)$_2$CuCl$_4$·H$_2$O. (a) [CuCl$_4$·H$_2$O]$_2$ dimers coupled into a chain by amino groups of aminoacridine (Aacr) molecules. Hydrogen bonds are marked by dashed lines and the other rings of the acridinium cations are omitted for clarity. (b) Dimeric unit disposition in the triclinic crystal unit cell.

monomers that are indirectly linked into chains. These linkages alternate in the chain direction between two water molecules and two amino groups from two intermittent acridinium cations as shown in figure 1(a).

The hydrogen bonds in the chain appear to be relatively weak. The water molecules in the centrosymmetrical [CuCl$_4$ · H$_2$O]$_2$ dimer form asymmetrical bridges with Cl · · · H bonds of 0.2143 nm and 0.2484 nm, whereas hydrogen bonds of the acridine NH$_2$ group form nearly symmetrical bridges between dimers and have the lengths 0.2546 nm and 0.2571 nm. Also the piridinium hydrogen (see NH groups in figure 1(a)) are involved in H bonding, N–H · · · Cl $=$ 0.2267 nm allowing the acridinium cations to become bridges between tetrahedra of two different chains. There exists a single [CuCl$_4$ · H$_2$O]$_2$ dimer in the crystal unit cell with the dimer plane nearly parallel to the ac-plane as shown in figure 1(b).

EPR experiments under normal pressure were performed on a Bruker ESP380E spectrometer operating in CW mode at frequency 9.4–9.8 GHz over the temperature range 4.2–300 K using an Oxford CF-935 flowing helium cryostat. High pressure EPR measurements at various temperatures were performed on a Radiopan SE/X-2547 spectrometer with hydrostatic pressure up to 400 MPa using a high pressure chamber and corrundum TE$_{112}$ resonator described previously [8].

The angular dependences of the EPR spectra were recorded in the three orthogonal planes of the **1**, **2**, **3** reference frame related to the crystal habit with $\mathbf{1} \equiv (01\bar{1})$, $\mathbf{3} \equiv [111]$ and $\mathbf{2} = \mathbf{3} \times \mathbf{1}$ as shown in the inset of figure 2.

The EPR spectra consist of a single Lorentzian resonance line in all crystal orientations below 140 K, whereas the line splits at higher temperatures. The angular variations at room temperature are shown in figure 2. The line positions (points) were fitted to the equation $g^2(\theta) = \alpha + \beta \cos 2\theta + \gamma \sin 2\theta$ (solid lines) in the three planes and the resulting g^2-tensor was diagonalized. The g-factors are temperature independent and parameters derived from

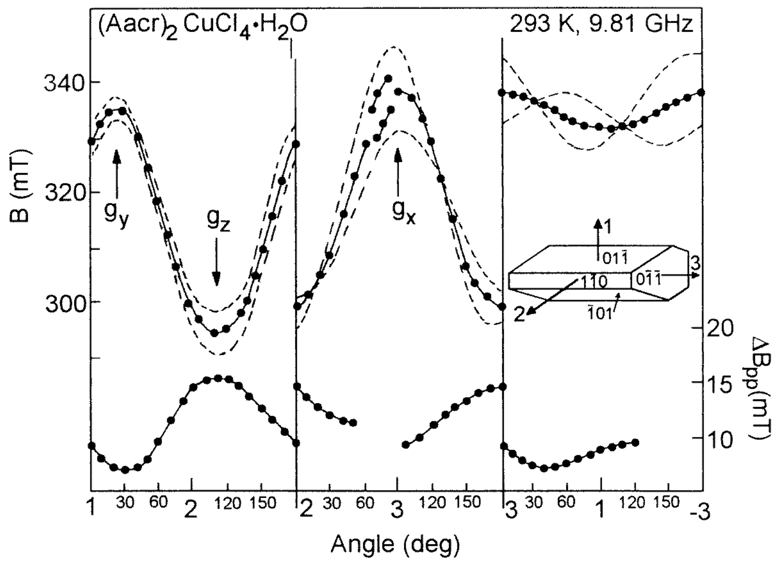

Figure 2. Angular variations of resonance field B and peak-to-peak linewidth ΔB_{pp} at room temperature. The solid lines in $B(\theta)$ plots superimposed on experimental points are the best fit to the $g^2(\theta)$ tensor equation (except the region where lines are split in the 2,3-plane). Dashed lines present the calculated zero-field splitting expected where no interdimer exchange operates in the crystal (see text). The solid lines in $\Delta B_{pp}(\theta)$ plots are guides for the eye only and experimental points are shown for those orientations where the well defined single line is observed. The inset shows the crystal habit with EPR orthogonal reference system **1**, **2**, **3**: **1** $\equiv$ $(01\bar{1})$, **3** $\equiv$ [111], **2** $=$ **3** $\times$ **1**.

Table 1. The g-factors, direction cosines and linewidth at 293 K.

	Direction cosines in **1**, **2**, **3**-frame			
g-factor	**1**	**2**	**3**	ΔB_{pp} (mT)
$g_z = 2.375(2)$	−0.3746	+ 0.9272	0	15.7(2)
$g_y = 2.090(2)$	+ 0.9272	+ 0.3746	0	7.3(2)
$g_x = 2.075(2)$	0	0	+ 1	11.0(8)

rotational data of figure 2 are summarized in table 1. Since the two $CuCl_4^{2-}$ anions in the crystal unit cell are coupled into a centrosymmetric dimer thus there does not exist a misalignment of the local crystal field axes and calculated g-factors are molecular factors of individual $CuCl_4$ tetrahedrons.

3. Results and discussion

3.1. g-factors and $CuCl_4^{2-}$ tetrahedron deformation

The g-factor sequence indicates $d_{x^2-y^2}$ or d_{xy} ground state characteristic for D_{2d} crystal field symmetry of the flattened $CuCl_4$ tetrahedron [19] with a small deformation towards a lower symmetry. The deformation axis S_4 being the g-factor z-axis is determined by the bisector of the Cl_1–Cu–Cl_4 angle ($2\beta = 138°$) and Cl_2–Cu–Cl_3 angle ($2\beta = 140°$). The average bisector direction calculated from these two directions has direction cosines (−0.2970,

+0.9520, −0.0520) which are very close to the z-axis direction determined from the EPR measurements (see table 1) with the inclination angle of about 6° only. A deviation of the $CuCl_4^{2-}$ structure, described by the flattening angle $2\beta = $ Cl–Cu–Cl, from the ideal tetrahedral T_d symmetry ($2\beta = 109.48°$) or planar D_{4h} symmetry ($2\beta = 180°$) is an intrinsic property of the complex. It is determined by a balance between crystal field stabilization energy favouring square-planar geometry and the destabilizing effect of the repulsion between chlorine anions favouring flattened D_{2d} geometry [20].

It is well recognized that the $CuCl_4^{2-}$ geometry is very sensitive to even small structural changes. A linear increase in optical d–d band energy versus flattening angle β is well known [21] and is accompanied by an EPR g-factor shift towards lower values when β increases [19]. Planar $CuCl_4^{2-}$ ions show a significant red shift of the optical band maxima on warming as a result of an increase in the vibronic activity [22].

The structure of $CuCl_4^{2-}$ in our crystal is described by the flattening of angle $2\beta = 139°$, which is a typical value among weakly hydrogen bonded chlorocuprates [23]. This structure is unexpectedly very stable over the whole temperature range. The bond lengths and bond angles are practically the same at 123 K and 298 K and EPR g-factors are temperature independent. The stabilization of the $CuCl_4^{2-}$ structure over the whole temperature range seems to be due to an interaction with acridinium molecules via $NH_2 \cdots Cl$ and $NH \cdots Cl$ hydrogen bonds.

3.2. Zero-field splitting (ZFS)

The double water bridged dimer in $(Aacr)_2CuCl_4 \cdot H_2O$ is not only a structural unit but it is also a real magnetic dimer with a magnetic triplet state. It is generally not obvious since, for example, the structural dimeric units in the *cis*-Cu(glycine)$_2 \cdot H_2O$ crystal are not real dimers due to a strong interdimer exchange interaction [24]. The existence of the triplet state is proved by our EPR results. For some crystal orientations in the 2,3-plane a splitting of the resonance line appears above 140 K. Temperature variations of the spectrum observed along the crystal direction in the 2,3-plane at $\theta = 65°$, where nearly maximal line splitting appears, are shown in figure 3. The resonance line splits into a doublet of two identical resonance lines. The splitting increases with temperature and then unexpectedly starts to decrease above 220 K.

The direction of maximal splitting coincides well with the Cu–Cu direction, having direction cosines (−0.30727, +0.36744, −0.87782) in the **1**, **2**, **3**-frame indicating that the zero-field splitting of the triplet state results from the dipole–dipole coupling. It is confirmed by simple calculations assuming the point dipole approximation and zero-field splitting Hamiltonian $H_{ZF} = \boldsymbol{S} \cdot \boldsymbol{D} \cdot \boldsymbol{S}$. It gives the line splitting along the D-tensor z-axis $3D_z = 1.95g^2r^{-3} = 22.2$ mT $= 0.0216$ cm^{-1} for the intercopper distance $r = 0.73$ nm, whereas the experimental value of the splitting is 19.8 mT $= 0.0192$ cm^{-1}. It is quite a good agreement. The coincidence of the Cu–Cu direction and the D-tensor z-axis indicates that there does not exist a considerable contribution from anisotropic exchange to the D-tensor, although in some dimeric chlorocuprates the anisotropic exchange dominates [25]. The theoretical plots of the line position with zero-field splitting, as expected when no interdimer exchange operates in the crystal, are shown by dashed lines in figure 2. The linewidth value and its angular dependence are determined to some extent by unresolved zero-field splitting and this effect is superimposed on a broadening effect from unresolved hyperfine structure of individual Cu^{2+} ions visible as $\Delta B_{pp} \propto g$.

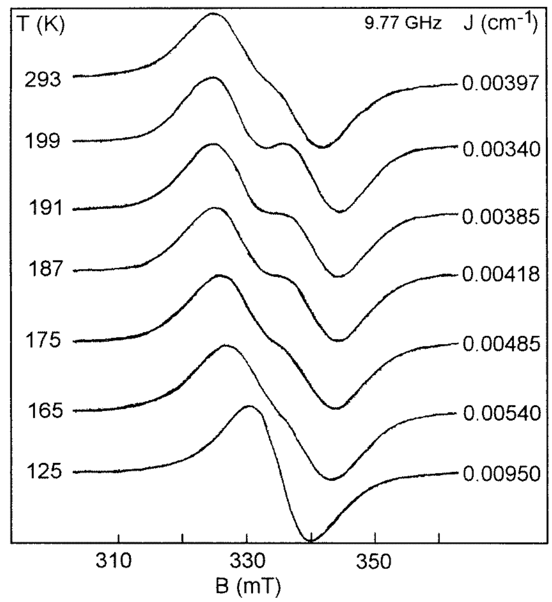

Figure 3. Temperature variations of the EPR spectrum observed in the 2,3-plane at $\theta = 65^\circ$ which is close to the z-axis of the zero-field splitting D-tensor. The simulated spectra with exchange coupling parameters J are perfectly superimposed on the experimental spectra.

3.3. Temperature and pressure effects

The g-factors are not affected by temperature indicating a stable $CuCl_4^{2-}$ structure whereas the zero-field splitting apparently varies with temperature. Positions of the ZFS doublet measured directly from the spectra for various temperatures are shown in figure 4(a) top. The lines coalesce completely at 140 K, although no phase transition exists in the crystal at this temperature. This effect is similar to the merging effect produced by exchange coupling between dimers in the $Cu(dien)Cl \cdot ClO_4$ crystal [26]. Thus, we suppose that the temperature dependent interdimer exchange coupling in our crystal can produce a merging effect of the zero-field splitting doublet lines.

A theoretical description of the merging effect can be made either in terms of the stochastic theories of magnetic resonance or by a modification of the Bloch equations. The former approach, based on the correlation functions and the relaxation matrix, is the most general treatment of the problem [27] and it was found to be useful in the case of isotropic single line EPR spectra and for hyperfine lines of radical centres in solutions [28]. In the case of exchange-type coupling between magnetically inequivalent sites of paramagnetic ions in single crystals, however, an appropriate solution can be found for the strong and weak exchange limits only [29]. A less sophisticated approach is based on the Bloch equations which are generalized to include a probability of spin jumping between two spin subsystems producing two resolved lines in an EPR spectrum. This approach has been originally applied for a description of chemical exchange effects in NMR spectra and in EPR spectra of solutions. In this case exact solutions of the appropriate Bloch equations exist in the weak and strong exchange limits and for zero-linewidth EPR spectra and can be found in textbooks [30, 31].

We have found [32, 33] a general analytical solution of the generalized Bloch equations for two-component EPR spectra of paramagnetic centres having different g-factors and linewidth

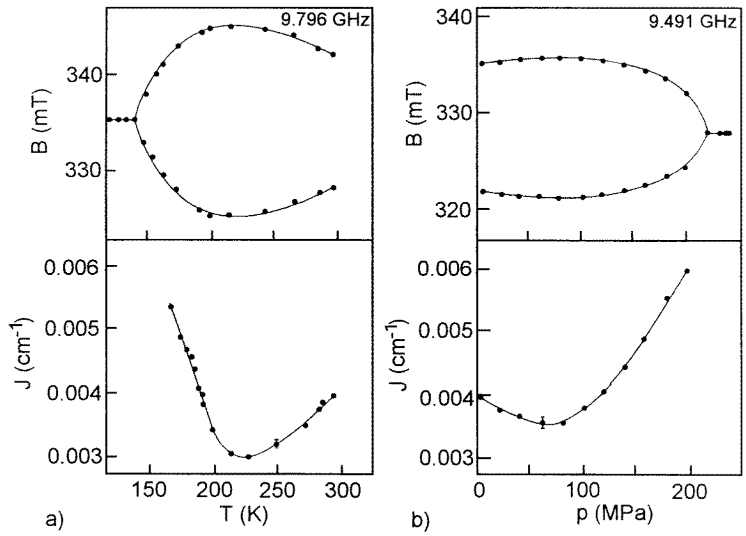

Figure 4. (a) Temperature variations of: (top) the resonance field of two lines arising from the zero-field splitting as measured directly from the spectra in the 2,3-plane at $\theta = 65°$; (bottom) interdimer exchange coupling parameter J derived from computer simulations using equation (1). (b) Pressure dependence of: (top) two line positions in magnetic field recorded at room temperature in the 2,3-plane at $\theta = 65°$; (bottom) interdimer exchange coupling parameter J. The solid lines are guides to the eye only.

$\Gamma = \sqrt{3}/2\Delta B_{pp}$, which is valid for the whole range of the exchange rate when the uncoupled lines have Lorentzian lineshape. This solution applied to the ZFS doublet with resonance fields B_1 and B_2, $B_0 = (B_1 + B_2)/2$ and linewidth Γ_1 and Γ_2, $\Gamma_0 = (\Gamma_1 + \Gamma_2)/2$, respectively, gives an EPR spectrum shape $Y(B)$ in the form:

$$Y(B) = N[\{[W_2 - 2(B - B_0)J](W_1^2 - W_2^2) - 4[(B - B_0)W_1 + (\Gamma_0 + J)W_2] \times[(B - B_0)W_2 + (\Gamma_0 + J)W_1]\}]/(W_1^2 + W_2^2) \quad (1)$$

where

$$W_1 = (B - B_1)(B - B_2) - (\Gamma_1 + K_1)(\Gamma_2 + K_2) + K_1K_2$$
$$W_2 = (B - B_1)(\Gamma_2 + K_2) + (B - B_2)(\Gamma_1 + K_1)$$

and $K_1 = JB_1/B_0$, $K_2 = JB_2/B_0$, where J is an exchange integral defined in the Hamiltonian $H_{ex} = |J|S_1S_2$. The N is a normalization factor proportional to the total number of paramagnetic ions in the sample and describes the intensity of the recorded experimental spectrum in the form of the first derivative $Y(B)$ of the absorption. All parameters are given in [mT] and the relationship between energy and field value of the exchange J is $J[\text{cm}^{-1}] = 0.466\,86 \times 10^{-3}g_0J$ [mT]. Using the above equations one can find the absolute value of J, since the merging effect goes in the same way independently if ferro- or antiferromagnetic coupling operates.

Computer simulations with the equation (1) have shown that the two-line spectra recorded at various temperatures and presented in figure 3 can be well reproduced with temperature independent splitting $(B_2 - B_1) = 17.5$ mT and the intrinsic linewidth linearly dependent on temperature with $\Delta B_{pp}^{(1)} = \Delta B_{pp}^{(2)} = 3.45$ mT at 293 K, and 3.75 mT at 171 K. The coupling parameter J varies with temperature as shown in figure 4(a) (bottom). The independence of

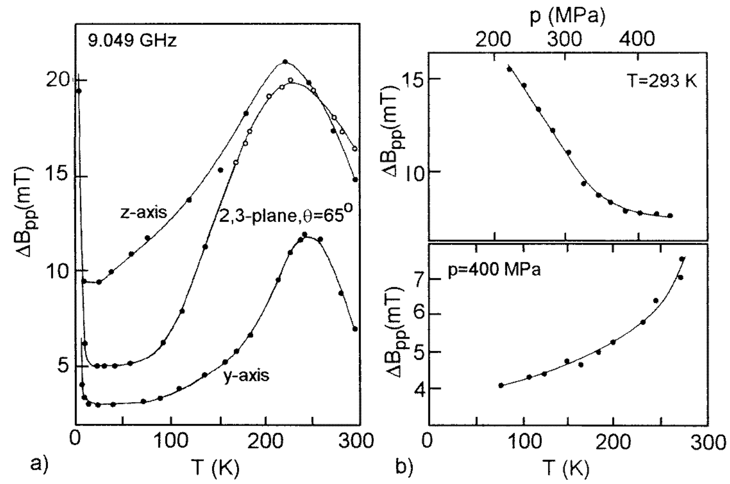

Figure 5. (a) Temperature dependence of the peak-to-peak linewidth along the g-tensor z-, y-axes and along the magnetic field direction in the 2,3-plane at $\theta = 65°$ which is close to the g-tensor x-axis of the $CuCl_4$ complex. The open circles are peak-to-peak splitting of the two resolved fine structure lines. (b) Line averaging process observed on the linewidth of the ZFS merged line above the merging point versus pressure at room temperature (top) and versus temperature under 400 MPa (bottom) for the crystal orientation: 2,3-plane $\theta = 65°$. The solid lines are guides for the eye only.

$(B_2 - B_1)$ from temperature is well understood. The dimer structure and local $CuCl_4$ structure are not affected by temperature, thus the zero-field splitting produced by dipolar coupling is temperature independent.

The determined J-value describes superexchange coupling between $[CuCl_4 \cdot H_2O]_2$ dimers mediated by hydrogen bondings with NH_2 group protons of the acridinium molecules. The coupling strongly increases on cooling below 220 K. It is the typical behaviour for the most of the weakly coupled copper(II) systems [7, 8, 26], while the minimum in $J(T)$-dependence at about 220 K and increase of J for higher temperatures are unusual. To check what is the mechanism responsible for such behaviour we have performed high pressure EPR experiments for the same crystal orientation as in temperature experiments (2,3-plane, $\theta = 65°$). The results shown in figure 4 show that increase in pressure acts like the decrease in temperature. Thus the observed $J(T)$-dependence is overdominated by thermal lattice contraction with negligible contribution from lattice dynamics.

In contradiction to the intrinsic linewidth determined from computer decoupling of the EPR lines, the experimentally observed linewidth is strongly temperature and pressure dependent as shown in figure 5. Thus, the apparent linewidth and lineshape are determined by the merging effect between ZFS lines even when the lines are not resolved, i.e., for $T < 220$ K (figure 5(a)) and $p > 200$ MPa (figure 5(b)) where ΔB_{pp} continuously decreases due to the increase in J. The ΔB_{pp}, being an effective linewidth of the fully averaged ZFS lines, decreases with temperature down to 70 K where it becomes temperature independent for most crystal orientations (see figure 5(a)). Below 10 K the ΔB_{pp} strongly increases on cooling, reaching $\Delta B_{pp} = 90$ mT at 4.2 K. This is a typical behaviour produced by precritical fluctuations, prior to a transition to an ordered magnetic state at low temperatures.

3.4. Phenomenological description of the $J(T)$ dependence

The $[CuCl_4 \cdot H_2O]_2$ dimer structure in $(Aacr)CuCl_4 \cdot H_2O$ is very stable as proved by the independence of the g-factors and zero-field splitting from temperature. Thus, the observed averaging effect of ZFS lines is dynamical in origin and the merging process is produced by variations of the interdimer superexchange coupling with temperature and pressure. Since we observed that increase in pressure works like decrease in temperature, thus the main driving mechanisms are the thermal lattice expansion and crystal compressibility similar to those we have identified in all copper(II) compounds studied so far [7]. The mechanisms suggest an increase in J-value on cooling and under pressure as a result of intermolecular bond shortening. This is the typical behaviour found in the vast majority of copper(II) salt crystals. The opposite behaviour was also observed [33], but in all cases a monotonic increase or decrease was observed. In our system, unexpectedly, a minimum in $J(T)$ appears at about 220 K and only below this temperature does a typical increase of J appear on cooling.

An opposite behaviour of $J(T)$, i.e., a decrease of observed $|J_{eff}|$ on cooling, can appear as a result of a competition between different contributions to J_{eff}, having different signs and different temperature behaviour. Moreover, at high temperature a phonon modulation of a superexchange pathway can produce $J(T)$-dependence. Atomic orbital overlapping modulated by thermal lattice vibrations depends, thus, on the average amplitude of atomic displacement which increases with temperature. Such a phonon mediated contribution will have the opposite sign, compared to the thermal lattice expansion effect, and will produce increase of J on heating. Such a contribution is overdominated, however, by the thermal expansion effect as is proved by the results of the high pressure experiment [8].

The EPR experiments allow us to measure an absolute value of effective superexchange integral (singlet–triplet splitting) which has positive ferromagnetic contributions J_F and negative antiferromagnetic contribution J_{AF}:

$$J_{eff} = J_F + J_{AF} \tag{2}$$

where

$$\begin{aligned} J_F &= J_{pot} + J_{double\text{-}spin\ polarization} \\ J_{AF} &= J_{kin} + J_{excited\ charge\ transfer\ configuration}. \end{aligned} \tag{3}$$

J_{pot} and J_{kin} are classical terms of superexchange defined in Anderson's solid state theory [2] as two terms in the following equation

$$J_{eff} = 2K_{12} + \frac{4b_{12}^2}{U}. \tag{4}$$

The K_{12} in the potential energy term contains the two-electron exchange integral between magnetic orbitals and the kinetic energy term contains the transfer integral b_{12} between two metal ions, and U is given as the difference of the Coulombic integrals $J_{11} - J_{22}$. In semiclassical orbital theories the potential energy term is identical as in equation (4), whereas kinetic energy has different forms. Hay *et al* [4] considered orbitals formed by unpaired electron localized on ionic $x^2 - y^2$ orbitals and found

$$J_{kin} = \frac{(E_1 - E_2)^2}{J_{11} - J_{22}} \tag{5}$$

where E_1, E_2 are energies of the magnetic orbital formed from $x^2 - y^2$ orbitals of metal ions. Kahn and Briat [3] in their molecular orbital formalism emphasize the role of the overlap between magnetic orbitals formed from metallic orbitals and have found

$$J_{kin} = 2S(\Delta^2 - \delta^2)^{1/2} \tag{6}$$

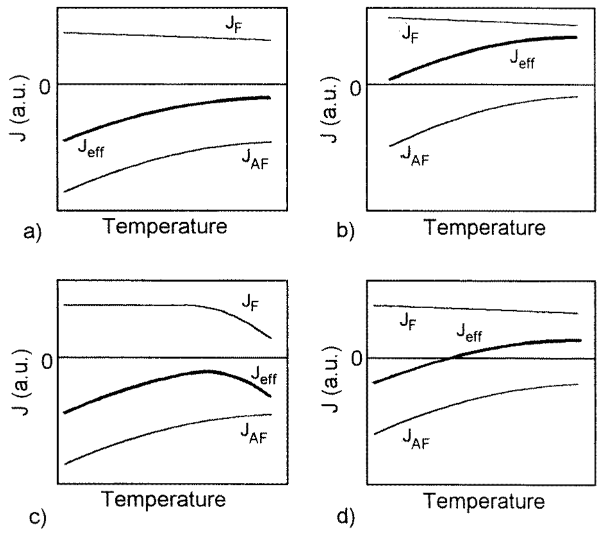

Figure 6. Possible temperature variations of the effective interdimer superexchange coupling J_{eff} resulting from various ferromagnetic (J_F) and antiferromagnetic (J_{AF}) dependences on temperature.

where S is the overlap integral between magnetic orbitals, Δ is the energy gap between two molecular orbitals built from metallic orbitals and δ is an energy difference between free ion orbitals in non-symmetrical dimers. The general conclusion from molecular orbital theories is that kinetic exchange gives an antiferromagnetic contribution to the exchange integral and is primarily determined by the overlap between magnetic orbitals and in the first order $J_{AF} \propto S^2$. It was stressed that potential exchange giving the ferromagnetic contribution to J_{eff} is relatively insensitive to small geometrical changes of dimer structure, whereas J_{AF} is rather sensitive to the changes though $E_1 - E_2 = \Delta$ [34, 35].

The molecular orbital theories include some excited orbital configurations of dimers, but effects of the spins of the bridged atoms or molecules are generally omitted. Such effects are explicitly included in *ab initio* calculations of exchange coupling in dimeric units, where various mechanisms of the configuration interaction (CI) are included. Among them, the double-spin polarization and excited charge transfer configurations give the most important contributions to J_{CI} and they are explicitly written in equations (3). The double-spin polarization, being a simultaneous flip of spins on the metal centres and the spins (with opposite direction) in the ligand, can give a positive contribution to J_{eff} although much smaller than J_{pot} [5, 36], whereas other CI contributions to J_{eff} are negative. Detailed *ab initio* calculations of a model dimeric centre with varying nature of the bridging atoms and different bridge length confirmed that the J_{pot}-contribution is not very sensitive to the geometrical changes, whereas J_{kin} is very sensitive to the distance being a nearly linear function of the fourth power of the overlap between bridge atomic orbitals and magnetic ionic orbitals [37].

The existing superexchange theories do not consider a possible influence of temperature or pressure either on J_{eff} or on a specific superexchange mechanism but allow us to conclude rather qualitatively about variations of the mechanism effectivity with geometry changes of simple dimeric units. So, we are able to predict qualitatively the relative changes of the four contributions to J_{eff} specified in equation (3) which are produced by interatomic distance shortening due to thermal contraction of a crystal lattice. We claim that all the temperature variations of J_{eff} observed by EPR, not only decrease or increase on heating, but also the non-monotonic behaviour, as in our crystal, can be explained as due to the thermal lattice contraction with a minor contribution from lattice dynamics as suggested by high pressure EPR measurements. We assume, according to the above theoretical descriptions, that J_{pot} does not vary or weakly decreases on heating, whereas J_{AF} and $J_{double\text{-}spin\ polarization}$ decrease when temperature increases. The possible $J_{eff}(T)$ variations are shown in figure 6. The typical decrease of J_{eff} on heating observed when J_{AF} dominates is shown in figure 6(a). A less common increase in J_{eff} is shown in figure 6(b). The possible non-monotonic $J_{eff}(T)$-dependences are presented in figures 6(c) and 6(d).

Our experimental $J(T)$-variations (figure 4) can be explained as in figure 6(c), i.e. assuming that the $J_{double\text{-}spin\ polarization}$ contribution decreases in the high temperature range. Although this is only a qualitative explanation and the various contributions to J_{eff} cannot be separated we can conclude that J_{eff} is antiferromagnetic in the whole temperature range. It should be stressed that a direct determination of the sign of J_{eff} is not possible by any method for such small J-values as measured by the EPR merging effect.

One can expect that the electron spin–lattice relaxation can give a contribution to the observed merging effect influencing the calculated J_{eff}-value at high temperatures where the relaxation is relatively fast. This seems to be not the case in our crystal, since the significant linewidth broadening should be simultaneously observed whereas the individual lines rather narrow on heating.

4. Conclusions

EPR allowed us to prove that water bibridged dimers of $CuCl_4^{2-}$ in the (9-amino-acridinium)$_2$CuCl$_2$ · H$_2$O crystal are real magnetic dimers with EPR detected zero-field splitting of the $S = 1$ state. The dimers are coupled into the chains and the superexchange coupling parameter varies anomalously with temperature, showing a decrease of the exchange integral below 220 K and an atypical increase above this temperature. A phenomenological model based on various temperature dependences of the competing contributions to the effective superexchange coupling shows that the observed $J(T)$-dependence with a minimum at $T = 220$ K can be explained as due to the thermal lattice expansion. The model predicts, simultaneously, that the observed superexchange coupling is antiferromagnetic in the whole temperature range.

References

[1] Kahn O 1993 *Molecular Magnetism* (New York: VCH)
[2] Anderson P W 1963 *Solid State Physics* vol 14, ed F Seitz and O Turnbull (New York: Academic) p 99
[3] Kahn O and Briat B 1976 *J. Chem. Soc. Faraday Trans.* II **72** 268
Kahn O and Briat B 1976 *J. Chem. Soc. Faraday Trans.* II **72** 1441
[4] Hay P J, Thibeault J C and Hoffmann R 1975 *J. Am. Chem. Soc.* **97** 4884
[5] de Loth P, Daudey J-P, Astheimer H, Walz L and Haase W 1985 *J. Chem. Phys.* **82** 5048
[6] Willet R D, Gatteschi D and Kahn O (eds) 1985 *Magneto-Structural Correlations in Exchange Coupled Systems* (Dordrecht: Reidel)
[7] Hoffmann S K, Hilczer W and Goslar J 1994 *Appl. Magn. Reson.* **7** 289
[8] Hoffmann S K, Krupski M and Hilczer W 1993 *Appl. Magn. Reson.* **5** 407
[9] Hoffmann S K, Hodgson D J and Hatfield W E 1985 *Inorg. Chem.* **24** 1194
[10] Yoneda H and Kida S 1960 *J. Am. Chem. Soc.* **82** 2139
[11] Bertrand J A, Eller P G, Fujita E, Lively M O and van der Veer D G 1979 *Inorg. Chem.* **18** 2419
[12] Nieuwpoort G, Verschoor G C and Reedijk J 1983 *J. Chem. Soc. Dalton Trans.* 531
[13] Walz L, Paulus H and Haase W 1985 *J. Chem. Soc. Dalton Trans.* 1243

[14] Muhonen H 1986 *Inorg. Chem.* **25** 4692
[15] Colacio E, Costes J P, Kivekas R, Laurent J P and Ruiz J 1991 *Inorg. Chem.* **30** 1475
[16] Moreno J M, Ruiz J, Dominguez-Vera J M and Colacio E 1993 *Inorg. Chim. Acta* **208** 111
[17] Nepveu F, Gehring S and Walz L 1986 *Chem. Phys. Lett.* **128** 300
[18] ter Haar L W 1993 unpublished data
[19] Hoffmann S K and Goslar J 1982 *J. Solid State Chem.* **44** 343
[20] Demuynek J, Veillard A and Wahgren U 1973 *J. Am. Chem. Soc.* **95** 5563
[21] Gaura R M, Stein O, Willett R D and West D X 1982 *Inorg. Chim. Acta* **60** 213
[22] Riley M J and Hitchman M A 1987 *Inorg. Chem.* **26** 3205
[23] Willett R D 1991 *Coord. Chem. Rev.* **109** 281
[24] Hoffmann S K, Goslar J and Szczepaniak L S1988 *Phys. Rev.* B **37** 7331
[25] Gatteschi D, Goslar J, Hilczer W, Hoffmann S K and Zanchini C 1989 *Inorg. Chem.* **28** 3395
[26] Hoffmann S K, Towle D K, Hatfield W E and Chaudhuri P 1985 *Inorg. Chem.* **24** 1307
[27] Kubo R and Tomita K 1954 *J. Phys. Soc. Japan* **9** 888
[28] Currin J D 1962 *Phys. Rev.* **126** 1995
[29] Yokota M and Koide S 1954 *J. Phys. Soc. Japan* **9** 953
[30] Carrington A and McLachlan A D 1967 *Introduction to Magnetic Resonance* (New York: Harper and Row)
[31] Atherton N M 1973 *Electron Spin Resonance—Theory and Applications* (New York: Ellis Horwood)
[32] Hilczer W and Hoffmann S K 1988 *Chem. Phys. Lett.* **144** 199
[33] Hoffmann S K and Hilczer W 1991 *Inorg. Chem.* **30** 2210
[34] Geiser U, Gaura R M, Willett R D and West D X 1986 *Inorg. Chem.* **25** 4203
[35] Kahn O and Charlot M F 1980 *Nuov. J. Chim.* **4** 567
[36] Kettle S F A and Tsaparlis G R 1983 *J. Chem. Phys.* **78** 5004
[37] Hart J R, Rappé A K, Gorum S M and Upton T H 1992 *J. Phys. Chem.* **96** 6255